RSC Advances

RSC Publishing

PAPER

View Article Online
View Journal | View Issue

Unzipping oyster shell†

Cite this: *RSC Advances*, 2013, **3**, 3284

Ramiz A. Boulos,[a] Catalin Harnagea,[b] Xiaofei Duan,[c] Robert N. Lamb,[c] Federico Rosei[b] and Colin L. Raston*[ad]

Received 10th August 2012,
Accepted 21st December 2012

DOI: 10.1039/c2ra21763e

www.rsc.org/advances

A novel technique to extract nacre tablets (bricks) from molluskan shells using 'soft energy' ionic liquid based dissolution of the organic material (mortar) between the tablets rather than using high energy and potentially tablet-damaging ball milling processing has been developed. The tablets isolated from this 'unzipping' of the shell in the ionic liquid n-butyl-3-methylimidazolium hexafluorophosphate were structurally characterized using scanning electron microscopy (SEM), transmission electron microscopy (TEM) and atomic force microscopy (AFM). High resolution AFM combined with *in situ* SEM shows nanoparticles of calcium carbonate approximately 4–5 nm in diameter present at the interface between multiple tablets of pearl nacre where there is incomplete dissolution of the mortar in the ionic liquid.

Published on 21 December 2012 on http://pubs.rsc.org | doi:10.1039/C2RA21763E
Downloaded by CNR on 11 February 2013

Introduction

Over the past decade there has been an increase in the number of studies on natural biomineralization processes and the cloning and characterization of the key proteins involved in the nucleation and crystal growth of the associated inorganic material.[1–7] Nevertheless, it still remains a challenge of biomimetic fabrication to replicate the structure of biominerals,[8] and understanding these processes at a fundamental level is important for exploiting their exceptional properties, for example in cosmetics and implants.[3] Growing functional materials that mimic and exploit the unusual properties of the nacre shell are particularly sought after, however a working model for the biological construction of nacre has to be unveiled first. A physical model for molluskan shell construction at the molecular level proposed by Cartwright and Checa begins with the fabrication of the polysaccharide chitin (*N*-acetyl-2-glucosamine) that is secreted in liquid form by the animal into the extrapallial space between the mantle and the shell.[8] Above a certain concentration, the chitin in this space, which also contains the polysaccharides, proteins and minerals, starts to crystallize and forms the base on which the nacre subsequently grows.[8] The crystallized chitin then undergoes a transformation into a protein-coated membrane which promotes the deposition of $CaCO_3$ on the surface.[8] The mineralization then proceeds by forming amorphous calcium carbonate,[8,9] (ACC), which is considerably more soluble than the crystalline polymorphs of the compound,[10] and can thus act as a mobile source of the mineral. Upon reaching its target, ACC is then either transformed into calcite, as the main constituent in the prismatic layer, or aragonite as the main constituent in the nacreous layer.[11–13] The proteins are believed to have an effect on the transformation processes,[11–13] however their roles remain unclear.[3] Modifications in the molluskan shell proteins have been shown to have an effect on the shape, size and morphology of the inorganic material and can also alter the nature of the incorporated material by modifying the binding affinities of ions.[14–16] Recently the presence of stable prenucleation clusters of $CaCO_3$ of $\sim$2 nm in size has been established using ion potential measurements in combination with analytical ultracentrifugation.[17] This discovery challenges classical models in which the crystallization of $CaCO_3$ either follows the formation of ACC and its subsequent transformation into crystalline polymorphs or the direct creation of the crystalline polymorphs.[17–19] *In silico* experiments carried out by Demichelis *et al.* found that the aforementioned prenucleation clusters are made of an 'ionic polymer' with alternating Ca^{2+} and CO_3^{2-} ions with a dynamic topology in which chains, branches and rings of clusters are evident.[18] The presence of disordered, flexible and hydrated ionic polymers can explain the formation of prenucleation clusters as well as the classical formation of $CaCO_3$ crystalline forms.

The inorganic component of nacre consists mainly of aragonite tablets arranged in a brick-like fashion, with an organic matrix in between, acting as the so-called 'mortar', as shown in Fig. 1.[8] The latter is comprised of proteins, saccharides, lipids and nucleotides, and accounts for $\sim$5%

[a]*Centre for Strategic Nano-Fabrication, School of Chemistry and Biochemistry, The University of Western Australia, 35 Stirling Hwy, Crawley, W. A. 6009, Australia. E-mail: colin.raston@uwa.edu.au; Fax: +61 86488 8683; Tel: +61 86488 3045*
[b]*Institut National de la Recherche Scientifique, Energie, Materiaux et Telecommunications, 1650 Boul. Lionel-Boulet, J3X 1S2 Varennes (QC), Canada*
[c]*School of Chemistry, The University of Melbourne, 2/800 Swanston Street, Victoria, 3010 Australia*
[d]*School of Chemical and Physical Sciences, Flinders University, Bedford Park, South Australia 5042, Australia*

† Electronic supplementary information (ESI) available. See DOI: 10.1039/c2ra21763e

This journal is © The Royal Society of Chemistry 2013

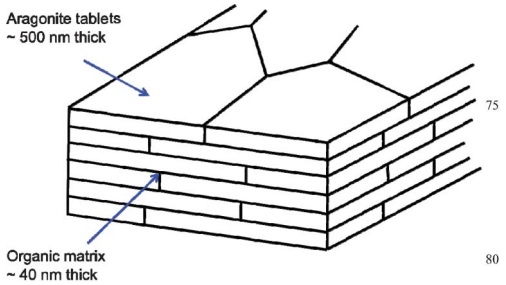

Fig. 1 Cartoon of the brick and mortar structure of nacre.

Published on 21 December 2012 on http://pubs.rsc.org | doi:10.1039/C2RA21763E
Downloaded by CNR on 11 February 2013

by weight of the nacre.[20–22] Gaining access to substantial quantities of the proteins in the matrix is necessary for their characterization and in developing their applications, for example in using them to control the nucleation and growth of other inorganic materials. Processes for this purpose need to operate under mild conditions to prevent denaturing the proteins, which typically occurs, for example, when using ultra high intensity grinding protocols [23,24] for disrupting the tablets to access the matrix. An alternative method is the use of acid digestion to dissolve the tablets and expose the matrix,[25] but this can also denature the proteins and generates a waste stream with a high calcium content which imposes a limitation on scaling up the process.

We report the development of a 'soft energy' mild extraction process operating at room temperature, using an ionic liquid to dissolve the organic matrix in pearl nacre. A recent study established that ionic liquids based on $BMIM^+$ with different counter anions affected the crystal shape but not the polymorph of $CaCO_3$, and revealed that there was no evidence of residual ionic liquid on the surface of the crystals after washing.[26] Thus our process employing ionic liquids has the potential to retain the integrity of the isolated nacre tablets, allowing an unprecedented characterization of undamaged tablets which we have undertaken using a range of techniques including transmission electron microscopy (TEM), scanning electron microscopy (SEM) and atomic force microscopy (AFM), and AFM combined with *in situ* SEM.

The ionic liquid of choice is the widely used hexafluorophosphate salt of n-butyl-3-methylimidazolium, [BMIM][PF_6], with imidazolium based ionic liquids being effective for a range of processes, including as solvent free media for enzyme catalyzed reactions.[27–31] This is important in the context of the process herein for ensuring that the proteins in the matrix retain their function. Also noteworthy is that these types of ionic liquids are effective in dissolving biopolymers, notably chitin,[32–34] which is present in the insoluble matrix of the nacre (mortar),[8] as well as a diverse range of small molecules.[35,36] Nanoparticles of $CaCO_3$ down to 4–5 nm are present at the interface between the tablets where there is incomplete dissolution with the ionic liquid, and on the surfaces of discrete tablets. These results are consistent with the findings of Bruet *et al.*,[37] and therefore the presence of these nanoparticles in the present study is not an artifact of the process.

Materials and methods

Shells of *Pinctada margaritifera* were provided by Pearl Technologies Pty Ltd, which were farmed in the pristine waters of the Abrolhos Islands in Western Australia. The decalcified organic conchiolin layer was removed by wet sand blasting of the shell followed by gentle brushing to remove any dust particles that might otherwise contaminate the samples. The shell was then crushed in a mortar and pestle, and initially 20 mL of [BMIM][PF_6] was added to 10 mg of the material in a 25 mL conical flask with subsequent stirring for 2 h. We later established that a similar result is obtained when 1 mL of the ionic liquid is used under the same conditions.

Sample preparation for analysis: the above mixture was centrifuged at 3220 × g for 20 min and the supernatant composed of the organic matrix in the ionic liquid was kept aside for future experiments, for a separate study targeting in the first instance the protein sequences and their quaternary crystal structures. The recovered $CaCO_3$ pellet was re-suspended in Milli Q water and the mixture centrifuged again at 3220 × g for 20 min. The supernatant was discarded and the resulting pellet re-suspended in Milli Q water and filtered under vacuum. The residue was collected and dried overnight in an oven at 70 °C, and then was quantitatively dispersed in water.

SEM measurements were recorded using a Zeiss 1555 VP-FESEM instrument operating at 15 KeV. The sample was dispersed in water and left to dry on a carbon tape mounted on a stub. X-ray elemental mapping was carried out using the same microscope at a working distance of 16 mm. TEM measurements were recorded using a 3000F JEOL instrument operating at 300 KeV. Energy dispersive spectroscopy (EDS) analysis was performed using the same microscope equipped with an Oxford Instruments INCA 200 EDS system. AFM images were recorded on a PicoScan system with a PicoScan 3000 picoSPM II controller utilized in tapping mode, with topographical images acquired using a grade 14 tapping mode cantilever. Samples were drop cast onto a freshly cleaved mica or graphite substrate and excess solution removed under vacuum. The intermediate stages of the extraction process were studied using a JEOL 4500 AFM/SEM equipped with an electron field emission gun and an SEM detector, operating in an ultrahigh vacuum (pressure 5×10^{-8} Pa). This system allowed easy location of the nacre particles, with a characteristic size of a few microns and an irregular shape, and enabled positioning of the AFM tip exactly on their surface, while preserving the tip sharpness. For these experiments, Vista tips purchased from Nanoscience Instruments with a resonance frequency of ~320 kHz and a tip radius below 10 nm were used. The AFM was operated in true non-contact mode (frequency shift feedback) at a set point of 50 Hz.

Published on 21 December 2012 on http://pubs.rsc.org | doi:10.1039/C2RA21763E
Downloaded by CNR on 11 February 2013

X-ray photoelectron spectroscopy (XPS) experiments were carried out on an ESCALAB220i-XL instrument from Thermo Scientific, UK. The background vacuum for analysis was below 7×10^{-9} mbar. A monochromated Al K alpha (energy 1486.6 eV) was used as the X-ray source at a power of 220 W (22 mA and 10 kV) and a spot size of 500 μm. A 90-degree angle was used as the photoelectron takeoff angle with a pass energy of 100 eV for survey scans (step size 1.0 eV). CasaXPS software was used for fitting the curves.

X-ray diffraction (XRD) was carried out on a Siemens D5000 Diffractometer using a fine-focus copper tube X-ray source. Experiments were conducted at an accelerating voltage of 35 kV and a current of 30 mA with the angles of incidence and reflection of the incident ray ranging from 20° to 80°. EVA software was used for visualizing and analyzing the output files.

Calcium analyses were carried out using a Thermo iCAP 6500 inductively coupled plasma atomic emission spectroscopy (ICP-AES) instrument. $CaCO_3$ purchased from Asia Pacific Specialty (APS) Chemicals Ltd. in powder form was added to Milli Q water and filtered through a 25 μm pore size filter paper. The residue was left to dry and 158 mg of the dried $CaCO_3$ was weighed and added to 5 mL of [BMIM][PF_6] in a Teflon beaker and stirred at room temperature for 2 h. The sample was centrifuged and the supernatant pipetted and filtered through a 0.2 μm pore size filter. The filtrate was diluted 40× with a 2% HNO_3 solution with 2 ppb Rh & Ir internal standard using a Hamilton Labs Autodiluter to produce 10 mL of diluted solution. Calcium levels were determined in the samples relative to a series of multi-element standards (0, 1, 2, 5 and 10 ppm in 5% HNO_3) by monitoring the 393.3 nm Ca line. Results were reported as a concentration in parts per million in the original sample following a diluent blank subtraction and dilution factor correction. XRD analysis showed that the $CaCO_3$ from APS Chemicals Ltd. used for the calcium analyses consisted of the calcite polymorph.

Thermogravimetric analysis (TGA) experiments were carried out in a Q50 Thermogravimetric Analyzer from 20 °C to 500 °C at a rate increase of 10 °C per minute.

Results and discussion

Molluskan shells are generally composed of three layers of material; an outer decalcified conchiolin layer, which was removed for this study, a prismatic layer and a nacreous layer. The prismatic layer is typically composed of 20–50 μm calcite crystals[38] which sit at right angles to the nacreous layer and are separated by an organic matrix approximately 5 μm thick.[39] The nacreous layer (nacre) is typically composed of pseudo-hexagonal, polygonal or rounded aragonite crystals approximately 5 to 20 μm in width and between 0.3 μm and 1.5 μm in height. Separating the aragonite crystals are organic 'bridges' (mortar) approximately 20 to 40 nm thick.[37] The shell from *Pinctada margaritifera* used in the study, was composed of 97.9% aragonite and 2.1% calcite as detected by XRD, shown in Fig. 2. Previous attempts to separate the prismatic and nacreous layers in the shell were successful, but the proposed process involved heating the shell at 400 °C for 18 h,[40] and it is therefore not applicable in developing processes for gaining access to the components of the mortar without destroying

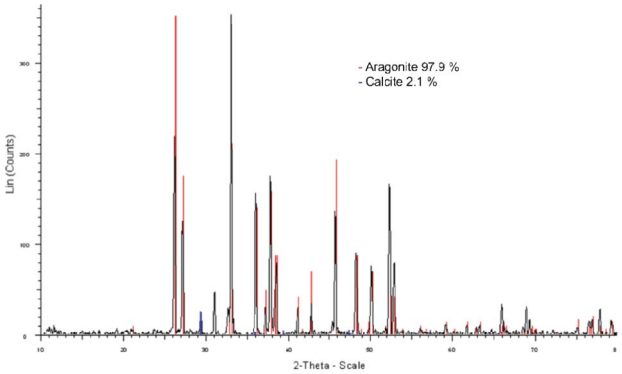

Fig. 2 XRD sample of the crushed shell prior to treatment with the ionic liquid [BMIM][PF_6]. The red line represents the aragonite profile and the blue line represents the calcite profile.

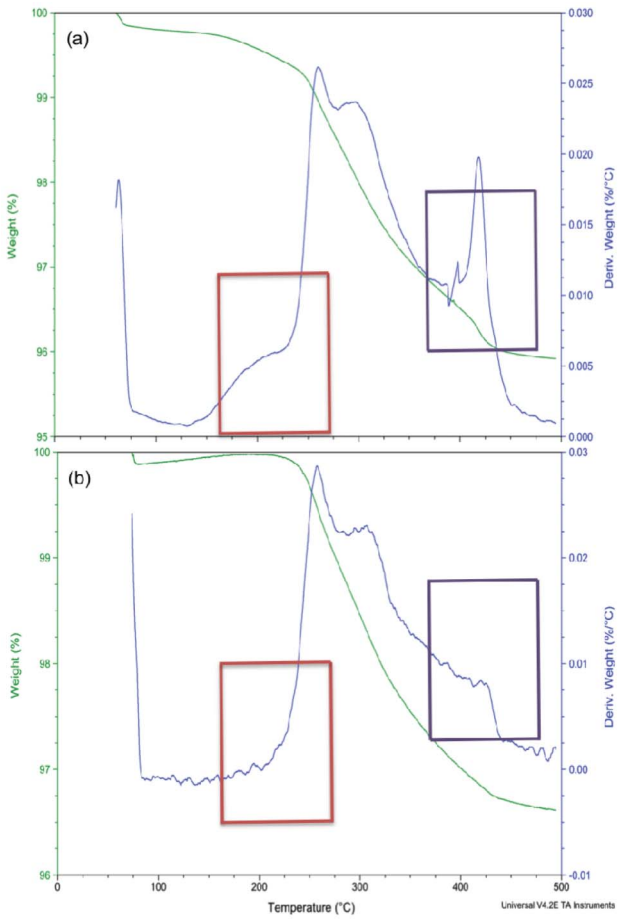

Fig. 3 TGA of the crushed shell prior to treatment, (a), and post treatment, (b), with [BMIM][PF_6].

This journal is © The Royal Society of Chemistry 2013

Published on 21 December 2012 on http://pubs.rsc.org | doi:10.1039/C2RA21763E
Downloaded by CNR on 11 February 2013

their integrity. For subsequent discussion, any reference to aragonite implies that there is likely to be a small amount of calcite present.

TGA data from the crushed shell prior to treatment with the ionic liquid, Fig. 3(a), showed ~4.13% weight loss upon heating, following three main derivative weight loss peak temperatures (Tp) at 200 °C (red box), 250 °C and 425 °C (purple box) corresponding to the largest weight change per unit temperature change. The weight loss at 200 °C corresponds to the vaporization of water from the crushed sample, whereas the weight losses at ~250 °C and at 425 °C correspond to the degradation of the organic matter in the sample.[41] After treating the crushed shell with the ionic liquid, the recovered tablets showed ~3.35% decrease in weight, Fig. 3(b). The difference between the two percentages accounts for ~18% and can be attributed to the amount of organic material solubilized by the ionic liquid. There is a decline in the 1st Tp at 200 °C (red box) after treatment with the ionic liquid, suggesting a reduced water-content in the sample. This finding is consistent with the dehydrating property that ionic liquids have, notably in reactions involving sugars such as glucose and sucrose, and in the extraction of the antimalarial Artemisinin.[42–45] In addition, there is a decrease in the 3rd Tp at 425 °C, which is consistent with the solubilization prowess of ionic liquids towards proteins and other organic material. Overall, these findings support a 'wetting' mechanism associated with solubilizing the organic matrix between the tablets, a task that is challenging at the nanometer scale.[46,47] As the ionic liquid absorbs water from the mortar, it is drawn further into the organic material thereby 'unzipping' the tablets.

A number of ionic liquids including 1-carboxymethyl-3-methylimidazolium bis(trifluoromethylsulfonyl)imide [HbetmIm][Tf_2N] have been described as 'supersolvents' capable of dissolving ionic salts like $Ca(OH)_2$.[48] While the cation in the ionic liquid in the present study does not have the complexing carboxyl group, the dissolution of $CaCO_3$ by [BMIM][PF_6] was examined using inductively coupled plasma atomic emission spectroscopy (ICP-AES). Less than 0.01 ppm of Ca^{2+} was detected, although the low solubility of the ionic liquid in water made it difficult to introduce the sample into the instrument reproducibly.

SEM images revealed tablets with different shapes and sizes (Fig. 4(a)), with such variation corresponding to different stages of crystal growth and curvature of the shell. Fig. 4(b)

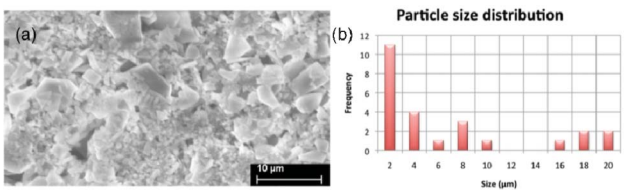

Fig. 4 (a) SEM micrograph of aragonite tablets after treating crushed nacre with [BMIM][PF_6], and (b) size distribution of tablets of diluted sample in water from (a).

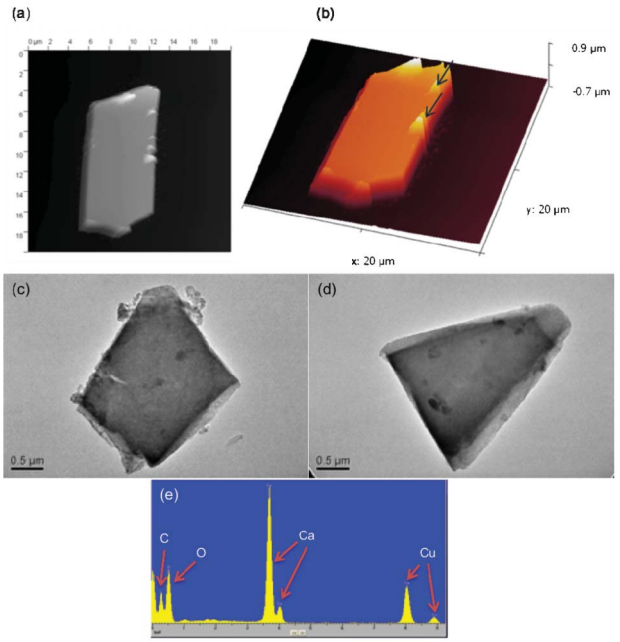

Fig. 5 (a) AFM image of an aragonite tablet post treatment with the ionic liquid, and (b) height profile of the aragonite tablet in (a). (c) and (d) are TEM images of different aragonite tablets showing nanoparticles, (e) elemental analysis of the aragonite tablet in (d).

shows the size distribution of tablets in a Milli Q water-diluted sample, revealing a dependence skewed to the left with the most frequent particle size being ⩽2 μm and the biggest particle size observed at ~20 μm. The AFM images in Fig. 5(a) and (b) show a 'mature' aragonite tablet that measures approximately 14 μm (l) × 6 μm (w) × 0.5 μm (h) which is consistent with the values from the literature.[49,50] Interestingly, there are aberrations on the surface (arrows pointing) such as cone-like protrusions, which give the nacreous layer its mechanical strength by interlocking with other tablets having similar features and creating resistance to sliding.[37,51] As observed from the TEM images in Fig. 5(c) and (d), the washed tablets recovered after treatment with the ionic liquid [BMIM][PF_6] have different shapes and sizes,[52,53] which are important in accommodating the curvature and varying thickness of the shell. EDS analysis of these tablets, Fig. 5(e), shows the presence of C, Ca and O peaks, as expected for the presence of the $CaCO_3$, and a Cu peak from the TEM grid itself. There were no peaks in the EDS corresponding to P and F from the ionic liquid and an absence of S and N peaks, both otherwise indicative of organic matter. In addition, no heavy metals were detected, as expected for oysters farmed in the pristine waters of the Abrohlos Islands. Elemental mapping of the tablets shows a uniform distribution of the elements Ca, C and O across the surface (Fig. S1, ESI†). EDS is an analytical technique that utilizes a high-energy X-ray beam that penetrates deep into the sample, rather than providing information on the outer layers/surface of the tablets, as in XPS for *ca* 10 nm depth. The XPS survey spectrum of the untreated sample in Fig. 6(a) shows the presence of Cl 2p, N 1s

Published on 21 December 2012 on http://pubs.rsc.org | doi:10.1039/C2RA21763E
Downloaded by CNR on 11 February 2013

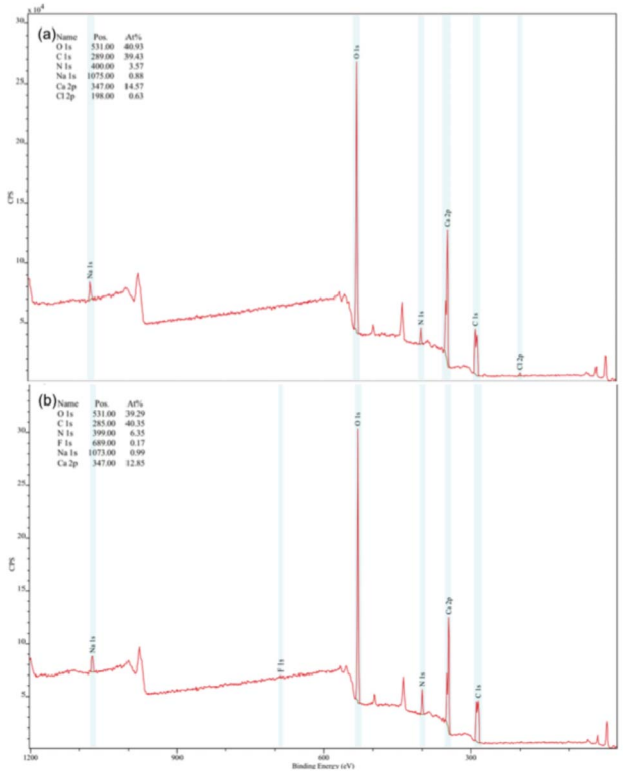

Fig. 6 XPS survey spectra of the crushed nacre before, (a), and after, (b) treatment with [BMIM][PF_6].

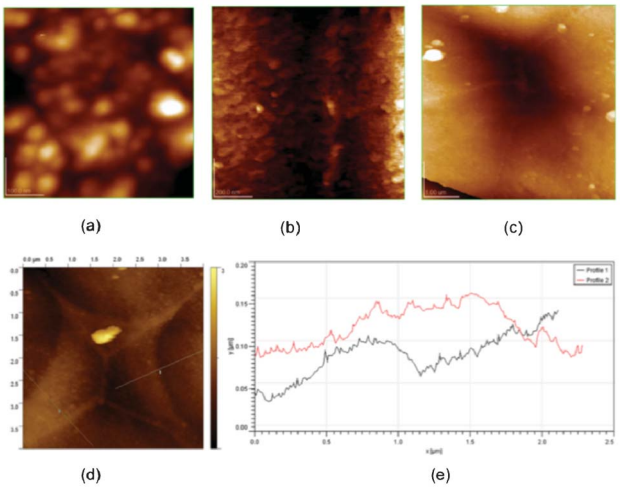

Fig. 7 (a) High resolution AFM image of the surface of aragonite tablets. (b) The region between two bricks, showing the formation of a crest. (c) An intersection region between several aragonite tablets, revealing the formation of a stalactitic feature. (d) Another joint region showing that the growth of a subsequent layer of inorganic material nucleates at the stalactite. (e) Height profiles along the lines shown in (d), evidencing a thickness of the laterally growing layer of 30–40 nm, Image sizes: (a) 500 nm, (b) 1 μm, (c) 5.5 μm (d) 4 μm.

and Na 1s peaks in addition to C 1s, Ca 2p and O 1s peaks arising from the $CaCO_3$. The atomic percentages (At%) of the Cl and Na were 0.88 At% and 0.63 At% respectively. Since the *Pinctada margaretifera* species grows in ocean water, the presence of these peaks is not surprising. The XPS survey spectrum of the [BMIM][PF_6^-] treated sample in Fig. 6(b) shows the absence of P but the presence of a F 1s peak with an atomic percentage of 0.17 At%, now with the absence of a Cl 2p peak. The presence of F arises presumably from the decomposition of PF_6^- and the high affinity of F^- towards Ca^{2+}, but no crystalline CaF_2 on the surface could be detected using X-ray powder diffraction. Previously N and S have been mapped in the growth-ring of nacre tablets in *Pinctada margaritifera* using NanoSIMS imaging for depth profiles between 90 nm and 160 nm,[54] but we could not confirm the presence of S using XPS. Moreover the absence of S herein is not contradictory to previous findings as the amount of organic material around the nacre tablets is significantly lower or even absent in tablets that have made contact with other neighboring tablets.[54]

The nacre tablets were also characterized by *in situ* combined SEM/AFM to identify their surface morphology and roughness, with the prospect of gaining insight into how the proteins reside on the surface and assemble the inorganic material. Combined SEM/AFM imaging allowed us to identify the interface between several aragonite bricks, as shown in Fig. 7. The image in Fig. 7(a) reveals that the surface of the bricks exhibits small particles (grains) with a lateral size varying between 5 and 100 nm, and a rms (root mean square) roughness of 5 nm over 1 μm^2 area. These 'grains' have been referred to previously as nanoasperites, a nacre tablet being composed of many grains[37] which accumulate and coalesce at the interface between aragonite bricks forming a crest, as shown in Fig. 7(b). At the joint region between several aragonite bricks, the intersection of the crests forms stalactite-like features (Fig. 7(c, d)). Upon reaching a height between 30 and 40 nm, a layer starts growing laterally from these stalactites, covering the aragonite bricks as seen in Fig. 7(d), with a growth speed higher along the crest, as suggested by the curvature of the step edge. The thickness of the growing overlayer is around 30–40 nm, comparable with the size of the largest grains (Fig. 7(e)) and the nucleation site of new layers occurs at the intersection of nacre tablets in the layer below, confirming previous reports.[54–56] The new tablets that are surrounded by organic matter then proceed to expand laterally until they meet the neighboring tablets fusing the organic rings together that subsequently disappear, enabling physical contact between nacre tablets and eventually forming a new layer.

Conclusions

We have established a simple procedure to separate the tablets from the organic matrix in shells of *Pinctada margaritifera* without affecting their integrity, which has potential for processing the shells of other oyster species. We use a less polar ionic liquid of the type previously used for the dissolution of chitin, *e.g.* 1-butyl-3-methyl-imidazolium chlor-

 This journal is © The Royal Society of Chemistry 2013

Published on 21 December 2012 on http://pubs.rsc.org | doi:10.1039/C2RA21763E
Downloaded by CNR on 11 February 2013

ide,[57] yet the ionic liquid used herein is effective in removing the organic material in the mortar, including the chitin. Our findings expand the ever-growing application base of ionic liquids, while providing an opportunity for studying all the components in pearl nacre using a processing approach that has a minimal effect on the isolated components. Combined SEM, TEM and AFM characterization reveals the structure of pristine aragonite crystals, with TGA suggesting a dewetting mechanism for the unzipping process. XPS is consistent with no residual ionic liquid on the surface, but with the presence of F^-, which arises from the decomposition of the PF_6^- anion of the ionic liquid. AFM combined with *in situ* SEM allowed the imaging of the interface between multiple aragonite bricks and to identify nanoparticles as small as 4–5 nm in size at the tablet surface. Future work will aim to improve the percentage of dissolved organic material using [BMIM][PF_6] as well as to investigate the effect of more benign ionic liquids, and devoid of a source of fluoride, for solubilizing the organic matter of the shell. In addition, the availability of the organic material from the mortar through room temperature processing under mild conditions offers scope for isolating quantities of the proteins, for then reverse engineering the formation of calcium carbonate bricks in a controlled way.

Acknowledgements

Funding from the Australian Research Council through the linkage program with support from Pearl Technology Pty Ltd is gratefully acknowledged. FR is grateful to the Canada Research Chairs program for partial salary support. CH acknowledges NSERC for a CGS scholarship. Work at INRS was sponsored by the Canada Foundation for Innovation and NSERC.

Notes and references

1 T. Furuhashi, I. Miksik, M. Smrz, B. Germann, D. Nebija, B. Lachmann and C. Noe, *Comp. Biochem. Physiol., Part B: Biochem. Mol. Biol.*, 2010, **155**, 195–200.
2 B. T. Livingston, C. E. Killian, F. Wilt, A. Cameron, M. J. Landrum, O. Ermolaeva, V. Sapojnikov, D. R. Maglott, A. M. Buchanan and C. A. Ettensohn, *Dev. Biol.*, 2006, **300**, 335–348.
3 J. S. Evans, *Chem. Rev.*, 2008, **108**, 4455–4462.
4 H. Miyamoto, F. Miyoshi and J. Kohno, *Zool. Sci.*, 2005, **22**, 311–315.
5 F. Marin, G. Luquet, B. Marie and D. Medakovic, *Curr. Top. Dev. Biol.*, 2008, **80**, 209–276.
6 P. Quinn, R. M. Bowers, X. Zhang, T. M. Wahlund, M. A. Fanelli, D. Olszova and B. A. Read, *Appl. Environ. Microbiol.*, 2006, **72**, 5512–5526.
7 P. Ramos-Silva, S. Benhamada, N. Le Roy, B. Marie, N. Guichard, I. Zanella-Cléon, L. Plasseraud, M. Cornelliat, G. Alcaraz, J. Kaandorp and F. Marin, *ChemBioChem*, 2012, **13**, 1067–1078.
8 J. H. E. Cartwright and A. G. Checa, *J. R. Soc. Interface*, 2007, **4**, 491–504.
9 N. Nassif, N. Pinna, N. Gehrke, M. Antonietti, C. Jäger and H. Cölfen, *Proc. Natl. Acad. Sci. U. S. A.*, 2005, **102**, 12653–12655.
10 M. D. Sikirić and H. F. Milhofer, *Adv. Colloid Interface Sci.*, 2006, **128–130**, 135–158.
11 L. Addadi, S. Raz and S. Weiner, *Adv. Mater.*, 2003, **15**, 959–970.
12 I. M. Weiss, N. Tuross, L. Addadi and S. Weiner, *J. Exp. Zool.*, 2002, **293**, 478–491.
13 N. Gerhke, N. Nassif, N. A. Pinna, M. H. S. Gupta and H. Colfen, *Chem. Mater.*, 2005, **17**, 6514–6516.
14 A. W. Maniccia, W. Yang, J. A. Johnson, S. Li. H. Tjong, H. Zhou, L. A. Shaket and J. J. Yang, *PMC Biophys.*, 2009, **2**, 11.
15 A. M. Belcher, X. H. Wu, R. J. Christensen, P. K. Hansma, G. D. Stucky and D. E. Morse, *Nature*, 1996, **381**, 56–58.
16 G. Fu, S. Valiyaveettil, B. Wopenka and D. E. Morse, *Biomacromolecules*, 2005, **6**, 1289–1298.
17 D. Gebauer, A. Völkel and H. Cölfen, *Science*, 2008, **322**, 1822.
18 R. Demichelis, P. Raiteri, J. D. Gale, D. Quigley and D. Gebauer, *Nat. Commun.*, 2011, **2**, 1–8.
19 D. Gebauer and H. Cölfen, *Nano Today*, 2011, **6**, 564–584.
20 M. Fritz and D. E. Morse, *Curr. Opin. Colloid Interface Sci.*, 1998, **3**, 55–62.
21 D. L. Kaplan, *Curr. Opin. Solid State Mater. Sci.*, 1998, **3**, 232–236.
22 F. H. Wilt, C. E. Killian and B. T. Livingston, *Differentiation*, 2003, **71**, 237–250.
23 C. Monder and P. Ramstad, *Arch. Biochem. Biophys.*, 1953, **46**, 376–384.
24 B. L. D'Appolonia and K. A. Gilles, *Cereal Chemistry*, 1967, **44**, 324–332.
25 D. Yang, P. Huang, B. Pan and Y. Mo, *Nano Biomed. Eng.*, 2010, **2**, 218–224.
26 Z. G. Hu, S. L. Song, J. J. Wang and L. Yang, *Chin. Chem. Lett.*, 2004, **15**, 707–710.
27 S. Bose, D. W. Armstrong and J. W. Petrich, *J. Phys. Chem. B*, 2010, **114**, 8221–8227.
28 J. K. Lee and M.-J. Kim, *J. Org. Chem.*, 2002, **67**, 6845–6847.
29 Y. H. Moon, S. M. Lee, S. H. Ha and Y.-M. Koo, *Korean J. Chem. Eng.*, 2006, **23**, 247–263.
30 U. Kragi, M. Eckstein and N. Kaftzik, *Curr. Opin. Biotechnol.*, 2002, **13**, 565–571.
31 M. Álvaro, E. Carbonell, B. Ferrer, H. Garcia and J. R. Herance, *Photochem. Photobiol.*, 2006, **82**, 185–190.
32 H. Xie, S. Zhang and S. Li, *Green Chem.*, 2006, **8**, 630–633.
33 Y. Wu, T. Sasaki, S. Irie and K. Sakurai, *Polymer*, 2008, **49**, 2321–2327.
34 K. Prasad, M.-a. Murakami, Y. Kaneko, A. Takada, Y. Nakamura and J.-i. Kadokawa, *Int. J. Biol. Macromol.*, 2009, **45**, 221–225.
35 L. Bédouet, F. Rusconi, M. Rousseau, D. Duplat, A. Marie, L. Dubost, K. Le Ny, S. Berland, J. Péduzzi and E. Lopez, *Comp. Biochem. Physiol., Part B: Biochem. Mol. Biol.*, 2006, **144**, 532–543.
36 G. Fu, S. R. Qiu, C. A. Orme, D. E. Morse and J. J. De Yoreo, *Adv. Mater.*, 2005, **17**, 2678–2683.
37 B. J. F. Bruet, H. J. Qi, M. C. Boyce, R. Panas, K. Tai, L. Frick and C. Ortiz, *J. Mater. Res.*, 2011, **20**, 2400–2419.
38 H. Liao, H. Mutvei, M. Sjöström, L. Hammarström and J. Li, *Biomaterials*, 2000, **21**, 457–468.

Published on 21 December 2012 on http://pubs.rsc.org | doi:10.1039/C2RA21763E
Downloaded by CNR on 11 February 2013

39 Y. Dauphin, *J. Biol. Chem.*, 2003, **278**, 15168–15177.
40 B. P. Bourgoin, *Mar. Environ. Res.*, 1988, **25**, 125–129.
41 C. M. Zaremba, D. E. Morse, S. Mann, P. K. Hansma and G. D. Stucky, *Chem. Mater.*, 1998, **10**, 3813–3824.
42 T. Ståhlberg, S. Rodriguez-Rodriguez, P. Fristrup and A. Riisager, *Chem.–Eur. J.*, 2011, **17**, 1456–1464.
43 C. Lansalot-Matras and C. Moreau, *Catal. Commun.*, 2003, **4**, 517–520.
44 C. Zhao, A. M. Bond and X. Lu, *Anal. Chem.*, 2012, **84**, 2784–2791.
45 M. W. Sanders, L. Wright, L. Tate, G. Fairless, L. Crowhurst, N. C. Bruce, A. J. Walker, G. A. Hembury and S. Shimizu, *J. Phys. Chem. A*, 2009, **113**, 10143–10145.
46 M. R. Powell, L. Cleary, M. Davenport, K. J. Shea and Z. S. Siwy, *Nat. Nanotechnol.*, 2011, **6**, 798–802.
47 L. Liu, J. Zhao, C.-Y. Yin, P. J. Culligan and X. Chen, *Phys. Chem. Chem. Phys.*, 2009, **11**, 6520–6524.
48 P. Nockemann, B. Thijs, T. N. Parac-Vogt, K. Van Hecke, L. Van Meervelt, B. Tinant, I. Hartenbach, T. Schleid, V. T. Ngan, M. T. Nguyen and K. Binnemans, *Inorg. Chem.*, 2008, **47**, 9987–9999.
49 H. K. Erben, *Biomineralization*, 1974, **7**, 14–27.
50 H. Nakahara, *Biomineralization & biological metal accumulation*, D. Reidel Publishing Co., Dordrecht, 1983.
51 R. Z. Wang, Z. Suo, A. G. Evans, N. Yao and I. A. Aksay, *J. Mater. Res.*, 2011, **16**, 2485–2493.
52 M. Suzuki, Y. Dauphin, L. Addadi and S. Weiner, *CrystEngComm*, 2011, **13**, 6780–6786.
53 A. G. Checa, T. Okamoto and J. Ramírez, *Proc. R. Soc. London, Ser. B*, 2006, **273**, 1329–1337.
54 M. Rousseau, A. Meibom, M. Géze, X. Bourrat, M. Angellier and E. Lopez, *J. Struct. Biol.*, 2009, **165**, 190–195.
55 K. Saruwatari, T. Matsui, H. Mukai, H. Nagasawa and T. Kogure, *Biomaterials*, 2009, **30**, 3028–3034.
56 M. Rousseau, E. Lopez, A. Couté, G. Mascarel, D. C. Smith, R. Naslain and X. Bourrat, *Key Eng. Mater.*, 2004, **254–256**, 1009–1012.
57 H. Xie, S. Zhang and S. Li, *Green Chem.*, 2006, **8**, 630–633.

 This journal is © The Royal Society of Chemistry 2013